Received: 18 December 2018 | Accepted: 7 January 2019 | Published on: 17 February 2019

DOI: 10.1002/ctpp.201800185

EDITOR'S CHOICE

Contributions to Plasma Physics

Benchmarking vdW-DF first-principles predictions against Coupled Electron–Ion Monte Carlo for high-pressure liquid hydrogen

Vitaly Gorelov[1] | **Carlo Pierleoni**[1,2] | **David M. Ceperley**[3]

[1]Maison de la Simulation, CEA, CNRS, Univ. Paris-Sud, UVSQ, Université Paris-Saclay, Gif-sur-Yvette, France

[2]Department of Physical and Chemical Sciences, University of L'Aquila, L'Aquila, Italy

[3]Department of Physics, University of Illinois, Urbana-Champaign, Illinois, USA

***Correspondence**

Carlo Pierleoni, Maison de la Simulation, CEA, CNRS, Univ. Paris-Sud, UVSQ, Université Paris-Saclay 91191 Gif-sur-Yvette, France.

Email: carlo.pierleoni@aquila.infn.it; carlo.pierleoni@cea.fr

Funding Information

This research was supported by the Agence Nationale de la Recherche, HyLightExtreme. National Science Foundation, OCI 07-25070. GENCI-CINES, 2018-A0030910282. State of Illinois. Fondation NanoSciences (Grenoble). DOE, NA DE-NA0002911.

We report first-principles results for the nuclear structure and optical responses of high-pressure liquid hydrogen along two isotherms in the region of molecular dissociation. We employ density functional theory with the vdW-DF approximation (vdW) and benchmark the results against existing predictions from Coupled Electron–Ion Monte Carlo (CEIMC). At fixed density and temperature, we find that the pressure obtained from vdW is higher than that from CEIMC by about 10 GPa in the molecular insulating phase and about 20 GPa in the dissociated metallic phase. Molecules are found to be over-stabilized using vdW, with a slightly shorter bond length and with a stronger resistance to compression. As a consequence, pressure dissociation along isotherms using vdW is more progressive than that computed with CEIMC. Below the critical point, the liquid–liquid phase transition is observed with both theories in the same density region, but the one predicted by vdW has a smaller density discontinuity, i.e. a smaller first-order character. The optical conductivity computed using Kubo–Greenwood formulation is rather similar for the two systems and reflects the slightly more pronounced molecular character of vdW.

KEYWORDS

high-pressure hydrogen, liquid–liquid phase transition, liquid structure, quantum Monte Carlo methods

1 | INTRODUCTION

Condensed hydrogen at high pressure is interesting because of the interplay between molecular dissociation and metallization in the liquid phase at high temperatures and between other phase transitions in the solid phase at lower temperatures.[1] First-principles methods are the main theoretical tools for investigating this system. The proximity of metallization and the dispersive character of the molecular interactions in the insulating phase have proven to be challenging for the well-established density functional theory (DFT)-based methods.[2–7] Predictions from various approximations are in qualitative agreement, but there are substantial quantitative differences, which makes it difficult to provide accurate predictions without benchmarking DFT results against more fundamental theories. At the same time, the simple electronic structure of hydrogen makes it the ideal candidate for developing new first-principles methods based on more fundamental many-body theories such as those based on quantum Monte Carlo (QMC) techniques. Two similar methods have appeared in the last decade and were applied to study compressed hydrogen: the Coupled Electron–Ion Monte Carlo (CEIMC)[2,8–10] and the quantum Monte Carlo molecular dynamics (QMCMD).[11,12] They are both based on solving the electronic problem by ground-state QMC methods but differ in the way they sample the nuclear configuration space.* The advantage of QMC over DFT is in its variational character: very different implementations of QMC, i.e. different forms of the many-body wave function, can be directly compared and ranked based on

© 2019 WILEY-VCH Verlag GmbH & Co. KGaA, Weinheim

https://doi.org/10.1002/ctpp.201800185

the value of their total energy.† After several attempts, these two methods are now in agreement about the occurrence and the location of the liquid–liquid phase transition (LLPT) in hydrogen.[12] This reinforces the idea that QMC can be used to assess the accuracy of DFT functionals for finite temperature predictions.

Previous detailed investigations of the accuracy of several DFT approximations against ground-state QMC for both crystalline and liquid static configurations[5] found van der Waals (vdW-DF)[13] and Heyd–Scuseria–Ernzerhof (HSE)[14] approximations to be the best candidates among the ones considered, with energy biases within fractions of mH/atoms and pressure biases within 10–20 GPa. A CEIMC investigation of the LLPT in hydrogen[10] confirmed these expectations: first-principles molecular dynamics (FPMD) with vdW-DF and HSE approximations predict LLPT transitions in closer agreement with the results from CEIMC than other approximations. Differences in the proton–proton pair correlation functions between CEIMC and FPMD are observed.[2,7,15] These differences can provide insight into the dissociation mechanism.

In this paper we compare the thermodynamics and local nuclear structure from first-principles simulations with vdW-DF and CEIMC, along two isotherms of hydrogen across the molecular dissociation region. These isotherms are above and below the critical temperature of the LLPT. A comparison of the optical conductivity within the Kubo–Greenwood (KG) framework is made. We only consider vdW-DF and disregard HSE since the computational requirements of HSE are much larger than those of vdW-DF while the expected accuracy is comparable.[5] Since the focus of this work is methodological, we limit our investigation to classical nuclei.

The rest of the paper is organized as follows. First, we briefly describe the methods employed in Section 2. Then we report our results for the thermodynamics and for the local nuclear structure in Section 3. In Section 4, we compare the optical conductivity and, finally, discuss the results and draw our conclusions.

2 | METHOD

In this paper, we use Metropolis Monte Carlo sampling for the nuclear degrees of freedom and, since the focus is on the accuracy of the potential energy surface, we limit our discussion to classical protons. The electronic energies used in the Metropolis sampling arise either from ground-state QMC in the CEIMC[1,8] or from ground-state DFT with the vdW-DF approximation. In both methods, the sampling is performed by a force-biased MC algorithm with DFT forces (DFTMC).[16] Given a nuclear configuration $\vec{R}$ of the N_{p} protons (here vectors are in the $3N_p$-dimensional space), a new configuration $\vec{R}'$ is proposed by a drifted random displacement according to

$$\vec{R}' = \vec{R} + h\vec{F}(\vec{R}) + \vec{\xi}, \tag{1}$$

where $\vec{F}(\vec{R})$ is the total force acting on the protons, h is an adjustable parameter with suitable dimensions, and $\vec{\xi}$ a Gaussian-distributed random vector with the properties

$$\langle \vec{\xi} \rangle = 0 \qquad \langle \vec{\xi}\ \vec{\xi}' \rangle = 2\, h\ \mathrm{k_B\ T}\ \mathbf{1}\ \delta_{\vec{\xi},\vec{\xi}'}, \tag{2}$$

where $\mathrm{k_B}$ is the Boltzmann constant, T the nuclear temperature, $\mathbf{1}$ is the identity matrix and $\delta_{\vec{\xi},\vec{\xi}'}$ indicates that the random noises at different steps are uncorrelated. Then the sampling probability is

$$G(\vec{R} \to \vec{R}'; h) \propto e^{-\frac{[\vec{R}' - \vec{R} - h\vec{F}(\vec{R})]^2}{4h\ \mathrm{k_B\ T}}}, \tag{3}$$

while the acceptance probability, satisfying detailed balance, is

$$A(\vec{R} \to \vec{R}') = \min[1, q(\vec{R} \to \vec{R}')] \qquad q(\vec{R} \to \vec{R}') = \frac{e^{-\beta E(\vec{R}')} G(\vec{R}' \to \vec{R}; h)}{e^{-\beta E(\vec{R})} G(\vec{R} \to \vec{R}'; h)}. \tag{4}$$

In the last equation, $E(\vec{R})$ is the total energy of the nuclear configuration $\vec{R}$ and $\beta = 1/\mathrm{k_B\ T}$. Within the DFT framework, this scheme can be used straightforwardly, and both forces and energies are from the DFT-vdW-DF functional. This strategy allows us to have a relatively high acceptance probability and also large moves even for a system of hundreds of protons, and hence an efficient sampling of the nuclear configurational space.

When solving the electronic problem with QMC, energy and forces have statistical noise, which must be taken into account to avoid bias in the sampling. In CEIMC, the noise over electronic energy is accounted for with the penalty method[8,17] while forces are not computed. Our present CEIMC implementation uses a two-level Metropolis scheme in which we first propose a new configuration according to the scheme described above based on DFT energy and forces, and if the new configuration $\vec{R}'$

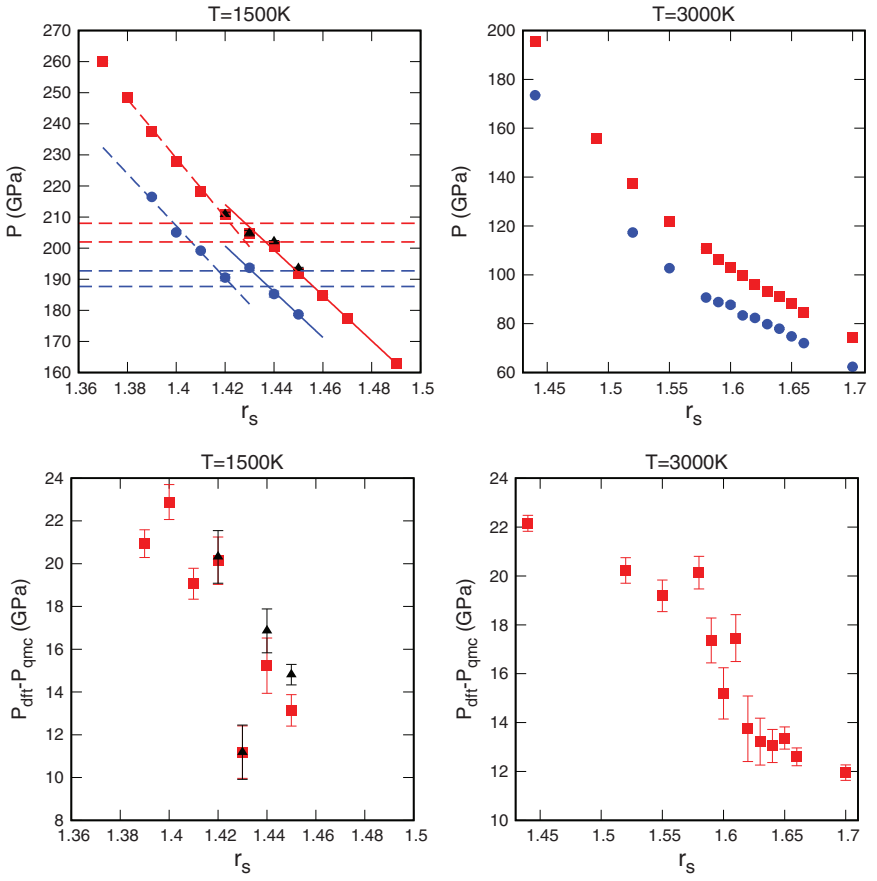

FIGURE 1 Equation of state along the two isotherms investigated. The upper panels report the pressure versus r_s from coupled electron–ion Monte Carlo (CEIMC) (blue circles) and from DFTMC with $N_p = 54$ (red squares). At $T = 1{,}500$ K, DFTMC for systems with $N_p = 128$ are reported (black triangles). In the lower panels, the difference between density functional theory (DFT) and quantum Monte Carlo (QMC) pressures is shown. Symbols are as in the upper panels

is accepted, we perform a second Metropolis acceptance test according to

$$A_2(\vec{R} \to \vec{R}') = \min[1, q_2(\vec{R} \to \vec{R}')] \qquad q_2(\vec{R} \to \vec{R}') = \frac{e^{-\beta E(\vec{R})}}{e^{-\beta E(\vec{R}')}} \, e^{-[\beta\delta(\vec{R}',\vec{R})+\beta^2 u(\vec{R}',\vec{R})]}, \tag{5}$$

where $\delta(\vec{R}', \vec{R})$ indicates the estimate of the difference between the QMC energies of configurations $\vec{R}'$ and $\vec{R}$, and $u(\vec{R}', \vec{R})$, a positive term, hence a penalty in the acceptance coming from the noise, can be replaced, to first approximation, by the estimate of the variance of the energy difference.[8,17]

We do not report new CEIMC calculations but use past calculations as a reference. Details about these calculations are reported in refs [10, 15, 18]. We do report new calculations using DFTMC employing the vdW-DF XC functional and the plane augmented-wave (PAW) method [19] with an energy cut-off of 40 Rydberg. In order to have a direct comparison with the CEIMC results, the DFT calculations have been performed with exactly the same protocol employed in CEIMC. Specifically, we carried out simulations of periodic systems of $N_p = 54$ protons, with a $4 \times 4 \times 4$ Monkhorst–Pack grid of k-points. This choice ensures that both results are affected by the same finite-size error at the single electron level. In CEIMC, many-body size effects are estimated and the thermodynamic results corrected accordingly.[10,20]‡ A further check that the residual finite-size effects in the DFT calculations are small is provided by direct comparison with calculations for a system of $N_p = 128$ protons, as detailed in the next section. The DFTMC calculations are performed with our in-house CEIMC code (BOPIMC), which uses the PWSCF[21] package as a DFT solver.

The electrical conductivity was computed using the KG[22,23] formula on 40 randomly selected configurations. The configurations are taken from DFTMC and CEIMC runs with $N_P = 54$ protons for a given density (ρ) and temperature (T). A post-processing tool in the QuantumEspresso suite[21] KGEC[24] was employed. For these calculations, we used an $8 \times 8 \times 8$ Monkhorst–Pack grid of k-points to get a better convergence in the low-ω part of the conductivity and included 48 bands to converge in the high-ω part up to $\omega \simeq 13$ eV.

3 | RESULTS

We performed simulations along two isotherms $T = 1{,}500$ and $3{,}000$ K, one below and one above the critical temperature of the LLPT. (The precise value of T_c is yet to be determined accurately.) In Figure 1 we compare the equation of state (EOS)

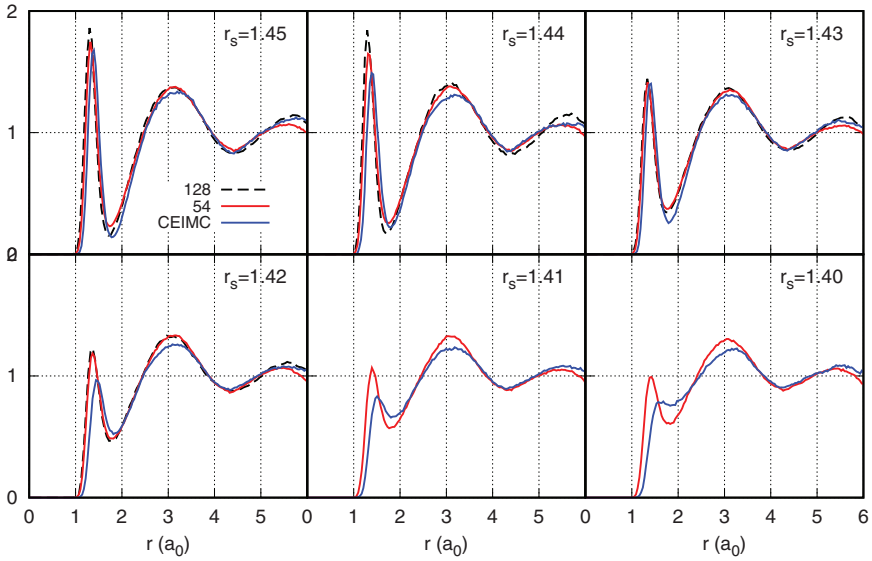

FIGURE 2 Proton–proton radial distribution functions along the $T = 1{,}500$ K isotherm. Comparison between coupled electron–ion Monte Carlo (CEIMC) (blue lines) and DFTMC-vdW-DF with $N_p = 54$ (red lines). At $r_s = 1.45,\ 1.44,\ 1.43,\ 1.42$, results for systems of $N_p = 128$ with DFTMC-vdW-DF are also reported (black dashed line)

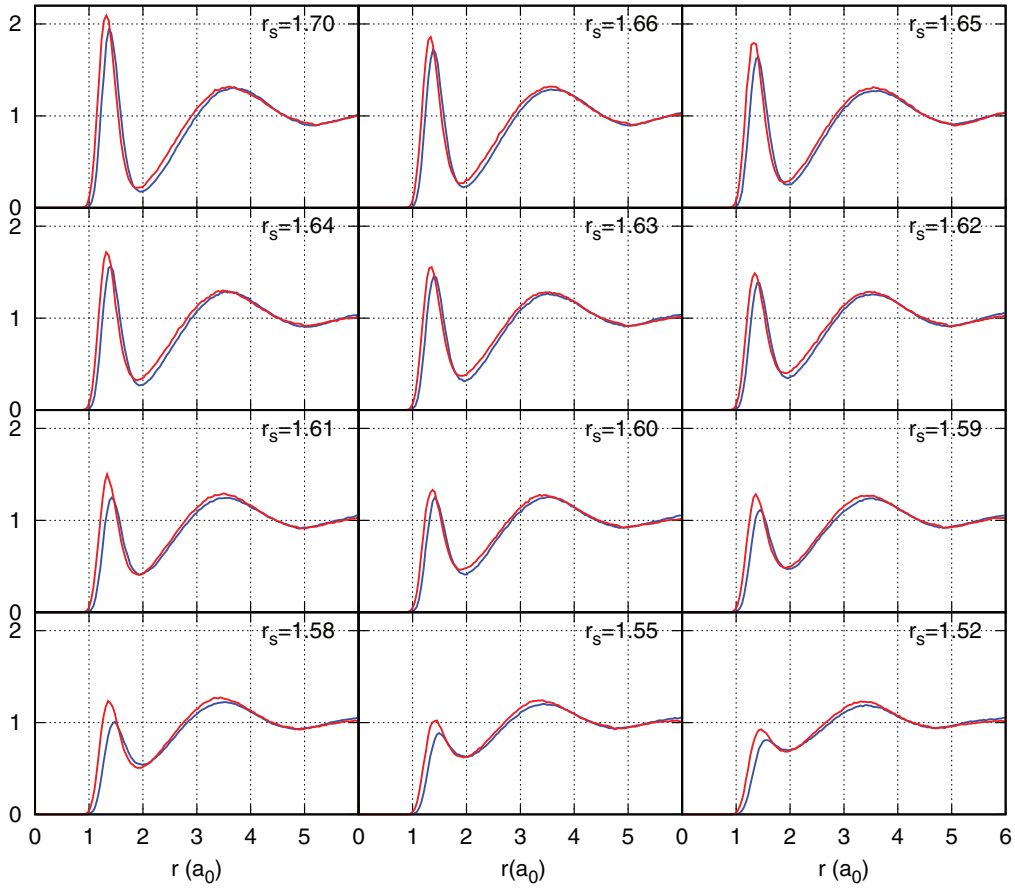

FIGURE 3 Proton–proton radial distribution function along the $T = 3{,}000$ K isotherm. Comparison between coupled electron–ion Monte Carlo (CEIMC) (blue lines) and DFTMC-vdW-DF with $N_p = 54$ (red lines)

along the two isotherms from CEIMC and from DFTMC-vdW-DF. The data shown in Figure 1 for CEIMC are from VMC and include finite-size corrections and RQMC corrections, as explained in the SM of ref. [10] (see also ref. [20]). The corresponding numerical values are given in the SM of ref. [10]. At the lower temperature, we observe a weakly first-order phase transition in both theories in the same range of densities. However, the width of the density plateau, obtained as the shift between the two branches of the EOS from fitting the data, is about two times larger in CEIMC than in DFT, signalling a stronger first-order character of the transition in QMC than in DFT. Residual finite-size effects, which could arise from the limited size of our systems, in particular at the phase transition, are negligibly small as shown in the upper left panel of Figure 1. The pressure from vdW-DF is always larger than that from CEIMC. Moreover, the accuracy of the vdW-DF predictions for the EOS is not uniform across molecular dissociation. This is shown in the two lower panels of Figure 1, where we report the difference between DFT and QMC pressures. At $T = 1{,}500$ K, molecular dissociation occurs suddenly between $r_s = 1.43$ and $r_s = 1.42$,

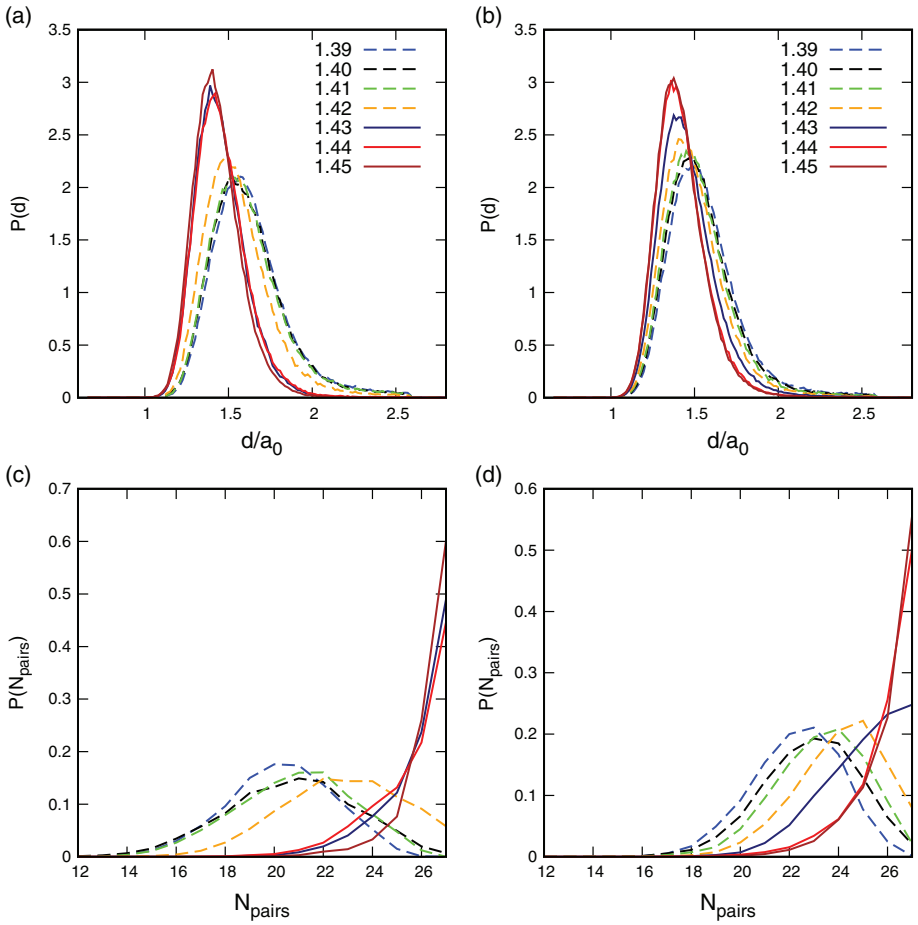

FIGURE 4 $T = 1{,}500$ K isotherm. Bond length distributions obtained with $r_c = 2.6$ (panels a and b) and the probability of the number of pairs at distance $r \leq 1.8a_0$ (panels c and d). coupled electron–ion Monte Carlo (CEIMC) results panels are (a) and (c); DFTMC results are panels (b) and (d)

where the pressure difference jumps from $\sim 10-14$ GPA to $\sim 20-22$ GPA. At $T = 3{,}000$ K, molecular dissociation, as well as the change in pressure difference, is more gradual with density. However, the observed pressure difference is in the same range of 12 GPa $\leq \Delta P \leq$ 22 GPa.

In Figure 2 we compare the proton–proton g(r) along the $T = 1{,}500$ K isotherm. We observe a qualitative agreement between the two theories, but data from DFTMC exhibit a more pronounced molecular character in the entire density range. The molecular bond length in DFTMC theory is slightly shorter than that in CEIMC, and the molecular dissociation is more progressive upon increasing density, in agreement with the smaller density discontinuity observed in the EOS. The same comparison along the $T = 3{,}000$ K isotherm is reported in Figure 3. Here, in both theories, the molecular dissociation is a progressive process. As before, the molecular peak is slightly shorter and the molecular character is slightly more pronounced (more correlation) in DFTMC than in CEIMC. The overall agreement is better than at the lower temperature.

In order to investigate in more detail the proton pairing in the system, we used a cluster algorithm to identify, for any given nuclear configuration, the number of bound pairs. A similar analysis for CEIMC had been already reported in ref. [15]. Specifically, given a proton, the algorithm looks for the closest proton that has not been already paired to another proton at shorter distance. The algorithm finds all such pairs within a given cut-off distance.

In the first analysis we used a large cut-off distance, $r_c = 2.6a_0$, in order to compute the bond length distribution without artificially cutting off the large distance tail. Results of this analysis for both CEIMC and DFTMC trajectories along the two isotherms are illustrated in the upper panels of Figures 4 and 5 where we report the bond distribution function. In each figure, the left panels correspond to the CEIMC results while the right panels to DFTMC. At $T = 1{,}500$ K, we see a change in behaviour for both theories at the LLPT, the discontinuity being more pronounced in CEIMC but still clearly visible in DFTMC.[§] In the molecular phase, the observed distribution is rather independent on the specific density, the maximum of probability is at $r = 1.40-1.42a_0$ in CEIMC and at $r = 1.36-1.38a_0$ in DFTMC, and the shape of the distribution is rather similar in the two methods. A similar difference in the molecular bond length between vdW-DF and QMC was previously observed in the crystalline state (see Figure 4 of ref. [5] and Figures 5 and 12 of ref. [18]). At densities beyond molecular dissociation, the bond distribution exhibits a more pronounced density dependence in both theories but remains slightly more localized in DFTMC than in CEIMC (the maximum of probability in DFTMC is at $r \sim 1.49a_0$ while it is at $r \sim 1.58a_0$ in CEIMC). At $T = 3{,}000$ K, a more progressive change of the bond distribution is observed over the investigated density range. The two theories have similar behaviour, but again the CEIMC results exhibit a stronger density dependence.

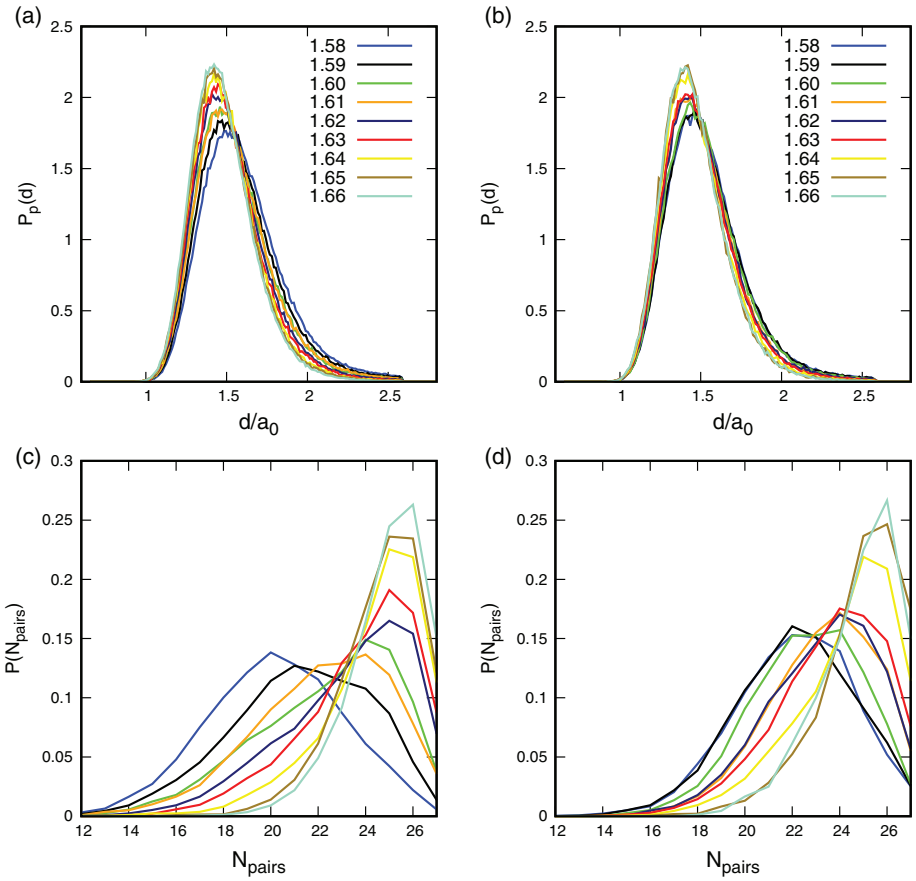

FIGURE 5 $T = 3{,}000$ K isotherm. Bond length distributions obtained with $r_c = 2.6$ (panels a and b) and the probability of the number of pairs at distance $r \leq 1.8a_0$ (panels c and d). Coupled electron–ion Monte Carlo (CEIMC) results panels are (a) and (c); DFTMC results are panels (b) and (d)

In the second analysis, we used a cut-off distance of $r_c = 1.8a_0$ (the first minimum of the $g(r)$) and computed the distribution in the number of the bonded pairs found within this cut-off. Results for both CEIMC and DFTMC along the two isotherms are illustrated in the lower panels of Figures 4 and 5. Also, this distribution exhibits a sudden change of shape at the LLPT along the $T = 1{,}500$ K isotherm, as seen in Figure 4. Again, the two theories are in qualitative agreement. More quantitatively, DFTMC shows a more localized distribution in the "dissociated" phase after the LLPT compared to CEIMC, and hence a stronger residual-associated character. At higher temperature, the change of the shape of the distribution with density is gradual in both theories. However, as observed at lower temperature, the CEIMC distributions become wider than the DFTMC distributions for increasing density signalling a less associated character.

4 | OPTICAL CONDUCTIVITY

Optical properties are relevant since they are the main source of experimental information at these high-pressure–high-temperature states of liquid hydrogen. In particular, recent experiments at The National Ignition Facility (NIF)[25] provided support for the LLPT lines predicted by CEIMC and FPMD-vdW-DF for deuterium on the basis of the optical response of the system.[¶] A subsequent investigation, within the KG framework, of optical properties across molecular dissociation supported experimental findings,[26] although other experiments suggest different scenarios[7] and the debate is still going on. For the purposes of the present benchmark, we believe it is interesting to check the sensitivity of the optical properties to the details of the local liquid structure. To this aim, we computed the optical conductivity at three distinct phase points, ($r_s = 1.45$, $T = 1,500$ K), ($r_s = 1.40$, $T = 1,500$ K), and ($r_s = 1.52$, $T = 3,000$ K) for liquid structure from both methods. At each state point and for each simulation method, we considered 40 independent nuclear configurations generated during the simulation run, and for each nuclear configuration we computed the optical conductivity with the KG single-electron formalism, assuming Kohn–Sham eigenstates from the vdW-DF XC functional. Details are given in Section 2. Statistical averages and errors are obtained over the sample of configurations. Figure 6a compares the real part of the average optical conductivity from CEIMC and from DFTMC-vdW-DF at the first state point, while Figure 6b reports the average electronic density of states from both theories. Results from the two methods are in good agreement, showing, once more, the similarity between the generated nuclear structures. However, we observe a slightly larger DOS at the Fermi level, which correlates with a slightly higher conductivity at small energies, from DFTMC-vdW-DF than from CEIMC. Conversely, around the maximum of conductivity at $\omega \sim 9$ eV,

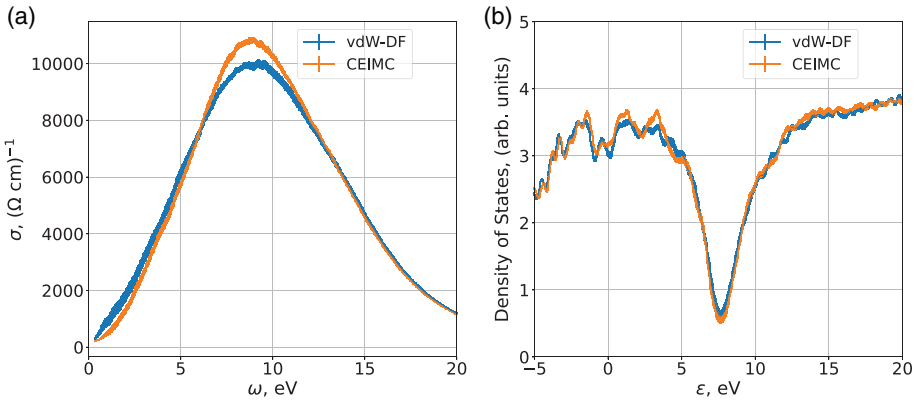

FIGURE 6 $T = 1{,}500$ K , $r_s = 1.45$. (a) Real part of the average optical conductivity from coupled electron–ion Monte Carlo (CEIMC) and DFTMC. (b) Average electronic density of states from CEIMC and DFTMC. Statistical errors are represented by the thickness of the lines

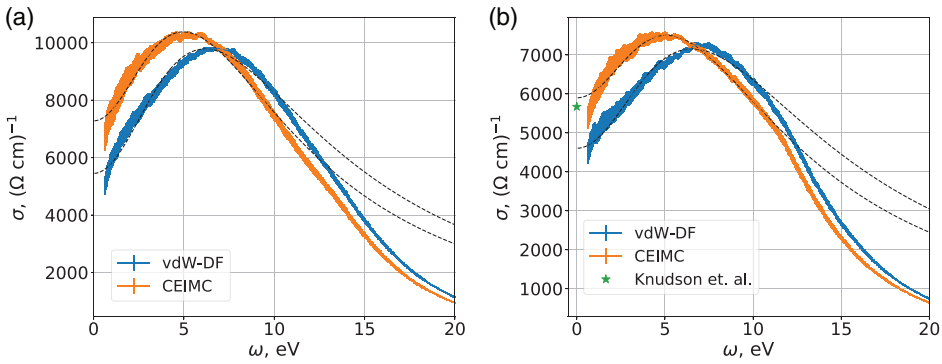

FIGURE 7 (a) Real part of the average optical conductivity at $r_s = 1.40$ and $T = 1{,}500$ K from coupled electron–ion Monte Carlo (CEIMC) and DFTMC. (b) Real part of the average optical conductivity at $r_s = 1.52$ and $T = 3{,}000$ K from CEIMC and DFTMC. Dashed lines represent a Drude–Smith fit to data. Statistical errors are represented by the thickness of the lines

CEIMC data are slightly higher than DFTMC-vdW-DF data. Note that this state point is at the edge of the metallic regimes: the energy gap is closed but the density of states at the Fermi level is rather small, resulting in a very small DC conductivity.

A similar analysis of the conducting regime is presented in Figure 7, where the optical conductivities for the other two investigated state points are reported. We observe similar comparisons at both state points: CEIMC conductivity is larger at small energies and the maximum is at a slightly lower energy than the DFTMC-vdW-DF one. This difference can be qualitatively justified as arising from the less "molecular" character of the CEIMC configurations (see Figures 2 and 3) and hence from a weaker electronic localization. Analysis of the conductivities in terms of the Drude–Smith model [27,28] provides $\sigma_{\mathrm{dft}}(\omega = 0) = 5,450(50)$, $\sigma_{\mathrm{qmc}}(\omega = 0) = 7,\ 280(70)(\Omega\ \mathrm{cm})^{-1}$ at $T = 1,\ 500$ K $r_s = 1.40$ and $\sigma_{\mathrm{dft}}(\omega = 0) = 4,\ 600\ (40)$, $\sigma_{\mathrm{qmc}}(\omega = 0) = 5,\ 900(40)(\Omega\ \mathrm{cm})^{-1}$ at $T = 3,\ 000$ K $r_s = 1.52$ for vdW-DF and CEIMC, respectively. In Figure 7b, we also report a recent result for the DC conductivity from FPMD with the vdW-DF XC approximation[29] at a state point close to our present one.‖

5 | CONCLUSIONS

In conclusion, we have presented a detailed comparison between CEIMC and DFTMC with the vdW-DF approximation for high-pressure liquid hydrogen across the interesting region where pressure-induced molecular dissociation occurs, either as a continuous process at high temperature or through a first-order phase transition at lower temperature. We have computed the EOS, the local nuclear structure of the fluid, and the optical conductivity at several state points. We observe that pressure from vdW-DF is higher than that from CEIMC by about 10 GPa in the molecular phase and about 20 GPa in the dissociated phase, indicating a loss of accuracy of the approximation upon molecular dissociation. Inspection of the local nuclear structure, as monitored by the proton–proton $g(r)$, shows that the molecular character of the fluid is more pronounced with DFTMC-vdW-DF and molecules have more resistance to compression and are more difficult to dissociate. Despite these quantitative differences, our investigation demonstrates, once again, the good quality of the vdW-DF functional to study high-pressure hydrogen in this interesting region of its phase diagram.

ACKNOWLEDGMENTS

V.G. and C.P. were supported by the Agence Nationale de la Recherche (ANR), France, under the program "Accueil de Chercheurs de Haut Niveau 2015" project: HyLightExtreme. D.M.C. was supported by a DOE Grant NA DE-NA0002911 and by the Fondation NanoSciences (Grenoble). Computer time was provided by PRACE Project 2016143296 and by an allocation of the Blue Waters sustained petascale computing project, supported by the National Science Foundation

(Award OCI 07-25070) and the State of Illinois, and by the HPC resources from GENCI-CINES under the allocation 2018-A0030910282.

ENDNOTES

∗ CEIMC samples the nuclear configuration space by Metropolis Monte Carlo, which requires computing electronic total energies, while QMCMD implements a Langevin dynamics based on electronic forces on the nuclei.
† The variance of the total energy is also an important quantity to compare since it decreases when the quality of the wave function is improved. Therefore a better wave function has a lower energy and a smaller variance.
‡ Many-body size effects on the local nuclear structure are negligible.
§ Convergence of results at the co-existence density is problematic since the system is observed to switch from one phase to the other several times during the simulation.
¶ The LLPT lines from CEIMC and from FPMD-vdW-DF are closer than the experimental resolution.
‖ The comparison is shown to support our present analysis. We believe that the value is slightly larger than our own because the density of that state point is slightly larger.

ORCID

Carlo Pierleoni https://orcid.org/0000-0001-9188-3846

REFERENCES

[1] J. M. McMahon, M. A. Morales, C. Pierleoni, D. M. Ceperley, *Rev. Mod. Phys.* **2012**, *84*, 1607.
[2] M. A. Morales, C. Pierleoni, E. Schwegler, D. M. Ceperley, *Proc. Natl. Acad. Sci.* **2010**, *107*, 12799.
[3] M. A. Morales, J. M. McMahon, C. Pierleoni, D. M. Ceperley, *Phys. Rev. B* **2013**, *87*, 184107.
[4] M. A. Morales, J. M. McMahon, C. Pierleoni, D. M. Ceperley, *Phys. Rev. Lett.* **2013**, *110*, 65702.
[5] R. C. Clay, J. McMinis, J. M. McMahon, C. Pierleoni, D. M. Ceperley, M. A. Morales, *Phys. Rev. B* **2014**, *89*, 184106.
[6] S. Azadi, W. M. C. Foulkes, T. D. Kuhne, *New J. Phys.* **2013**, *15*, 113005.
[7] M. D. Knudson, M. P. Desjarlais, A. Becker, R. W. Lemke, K. R. Cochrane, M. E. Savage, D. E. Bliss, T. R. Mattsson, R. Redmer, *Science* **2015**, *348*, 1455.
[8] C. Pierleoni, D. M. Ceperley, *Lecture Notes in Physics*, Springer, Berlin **2006**, p. 641.
[9] N. M. Tubman, E. Liberatore, C. Pierleoni, M. Holzmann, D. M. Ceperley, *Phys. Rev. Lett.* **2015**, *115*, 1.
[10] C. Pierleoni, M. A. Morales, G. Rillo, M. Holzmann, D. M. Ceperley, *Proc. Natl. Acad. Sci.* **2016**, *113*, 4954.
[11] C. Attaccalite, S. Sorella, *Phys. Rev. Lett.* **2008**, *100*, 114501.
[12] G. Mazzola, R. Helled, S. Sorella, *Phys. Rev. Lett.* **2018**, *120*, 025701.
[13] M. Dion, H. Rydberg, E. Schroder, D. C. Langreth, B. I. Lundqvist, *Phys. Rev. Lett.* **2004**, *92*, 246401-1.
[14] J. Heyd, J. E. Peralta, G. E. Scuseria, R. L. Martin, *J. Chem. Phys.* **2005**, *123*, 174101.
[15] C. Pierleoni, M. Holzmann, D. M. Ceperley, *Contrib. Plasma Phys.* **2018**, *58*, 99.
[16] M. P. Allen, D. J. Tildesley, *Computer Simulation of Liquids*, Oxford University Press, New York **1987**.
[17] D. Ceperley, M. Dewing, *J. Chem. Phys.* **1999**, *110*, 9812.
[18] G. Rillo, M. A. Morales, D. M. Ceperley, C. Pierleoni, *J. Chem Phys.* **2018**, *148*, 102314.
[19] P. E. Blochl, *Phys. Rev. B* **1994**, *50*, 17953.
[20] M. Holzmann, R. C. Clay, M. A. Morales, N. M. Tubman, D. M. Ceperley, C. Pierleoni, *Phys. Rev. B* **2016**, *94*, 035126.
[21] P. Giannozzi, O. Andreussi, T. Brumme, O. Bunau, M. Buongiorno Nardelli, M. Calandra, R. Car, C. Cavazzoni, D. Ceresoli, M. Cococcioni, N. Colonna, I. Carnimeo, A. Dal Corso, S. de Gironcoli, P. Delugas, R. A. J. DiStasio, A. Ferretti, A. Floris, G. Fratesi, G. Fugallo, R. Gebauer, U. Gerstmann, F. Giustino, T. Gorni, J. Jia, M. Kawamura, A. H-Y Ko, E. Kokalj, M. Kukukbenli, M. Lazzeri, N. Marsili, F. Marzari, N. L. N. Mauri, H.-V. Nguyen, A. Oreto-de-la Roza, L. Laulatto, S. Ponce, D. Rocca, R. Sabatini, B. Santra, M. Schlipf, A. Seitsonen, A. Smogunov, I. Timrov, T. Thonhauser, P. Umari, N. Vast, X. Wu, S. Baroni, *J. Phys. Cond Mat.* **2017**, *29*, 465901.
[22] R. Kubo, *J. Phys. Soc. Jpn* **1957**, *12*, 570.
[23] D. A. Greenwood, *Proc. Phys. Soc.* **1958**, *71*(4), 585.
[24] L. Calderín, V. V. Karasiev, S. B. Trickey, *Comput. Phys. Commun.* **2017**, *221*, 118.
[25] P. M. Celliers, M. Millot, S. Brygoo, R. S. McWilliams, D. E. Fratanduono, J. R. Rygg, A. F. Goncharov, P. Loubeyre, J. H. Eggert, J. L. Peterson, N. B. Meezan, S. Le Pape, G. W. Collins, R. Jeanloz, R. J. Hemley, *Science* **2018**, *361*, 677.
[26] G. Rillo, M. A. Morales, D. M. Ceperley, C. Pierleoni, *submitted* **2018**. arXiv:1810.08131
[27] N. V. Smith, *Phys. Rev. B: Condens. Matter Mater. Phys.* **2001**, *64*, 155106.
[28] T. L. Cocker, D. Baillie, M. Buruma, L. V. Titova, R. D. Sydora, F. Marsiglio, F. A. Hegmann, *Phys. Rev. B* **2017**, *96*, 205439.
[29] M. D. Knudson, M. P. Desjarlais, M. Preising, R. Redmer, *Phys. Rev. B* **2018**, *98*, 174110.

How to cite this article: Gorelov V, Pierleoni C, Ceperley DM. Benchmarking vdW-DF first-principles predictions against Coupled Electron–Ion Monte Carlo for high-pressure liquid hydrogen. *Contributions to Plasma Physics* 2019;59:e201800185. https://doi.org/10.1002/ctpp.201800185